Regeneration in Experimental Alveolar Bone Defect Using Human Umbilical Cord Mesenchymal Stem Cells

Akiko Toyota[1] , Rei Shinagawa[1], Mikiko Mano[1], Kazuyuki Tokioka[2], and Naoto Suda[1]

Abstract

Cleft lip and palate is a congenital disorder including cleft lip, and/or cleft palate, and/or alveolar cleft, with high incidence. The alveolar cleft causes morphological and functional abnormalities. To obtain bone bridge formation and continuous structure between alveolar clefts, surgical interventions are performed from infancy to childhood. However, desirable bone bridge formation is not obtained in many cases. Regenerative medicine using mesenchymal stem cells (MSCs) is expected to be a useful strategy to obtain sufficient bone bridge formation between alveolar clefts. In this study, we examined the effect of human umbilical cord-derived MSCs by transplantation into a rat experimental alveolar cleft model. Human umbilical cords were digested enzymatically and the isolated cells were collected (UC-EZ cells). Next, CD146-positive cells were enriched from UC-EZ cells by magnetic-activated cell sorting (UC-MACS cells). UC-EZ and UC-MACS cells showed MSC gene/protein expression, *in vitro*. Both cells had multipotency and could differentiate to osteogenic, chondrogenic, and adipogenic lineages under the differentiation-inducing media. However, UC-EZ cells lacked *Sox2* expression and showed the lower ratio of MSCs than UC-MACS cells. Thus, UC-MACS cells were transplanted with hydroxyapatite and collagen (HA + Col) into alveolar cleft model to evaluate bone formation *in vivo*. The results of micro computed tomography and histological staining showed that UC-MACS cells with HA + Col induced more abundant bone formation between the experimental alveolar clefts than HA + Col implantation only. Cells immunopositive for osteopontin were accumulated along the bone surface and some of them were embedded in the bone. Cells immunopositive for human-specific mitochondria were aligned along the newly formed bone surface and in the new bone, suggesting that UC-MACS cells contributed to the bone bridge formation between alveolar clefts. These findings indicate that human umbilical cords are reliable bioresource and UC-MACS cells are useful for the alveolar cleft regeneration.

Keywords

Introduction

Cleft lip and palate (CLP) is a group of conditions that include cleft lip, and/or cleft palate, and/or alveolar cleft[1]. CLP is a multifactorial disease and many genetic and environmental factors are known to be involved[2,3]. The incidence of CLP varies among various racial groups[1]. The incidence was reported to be 1 in 1,000 births in Caucasians, 1 in 2,500 births in those of African descent, and relatively high at 1 in 500 births in Asians[4–6].

CLP causes several morphological abnormalities in the maxillofacial regions, including lip, nose, dental arch, and palate[7,8]. Besides these morphological problems, CLP causes various functional problems, e.g., feeding disorder in infants, masticatory and occlusal disorders, speech problems, and otopathology[9–12]. To correct these problems, surgical correction of the lip, palate, and alveolus must be

[1] Division of Orthodontics, Department of Human Development and Fostering, Meikai University School of Dentistry, Saitama, Japan
[2] Department of Plastic and Reconstructive Surgery, Saitama Medical University, Saitama, Japan

Corresponding Author:
Akiko Toyota, Division of Orthodontics, Department of Human Development and Fostering, Meikai University School of Dentistry, 1-1 Keyakidai, Sakado, Saitama 350-0283, Japan.
Email: akiko25@dent.meikai.ac.jp

planned. Cheiloplasty is usually performed at 3 to 6 months after birth to help the suckling of CLP infants[13–15]. Palatoplasty is usually arranged before utterance to avoid speech abnormality[16,17]. For the surgical closure of the alveolar cleft, two types of surgical interventions are known[18–26]. The first intervention is the secondary bone graft (SBG) introduced by Boyne and Sands[18,19]. Classically, iliac bone grafts have been used to facilitate bone bridge formation[20,21]. SBG is usually performed in accordance with the permanent tooth eruption to promote normal tooth eruption at 5 to 10 years of age[22,23]. The second intervention is gingivoperiosteoplasty (GPP)[24–26]. GPP was introduced by Skoog as an alternative to SBG and was modified by Cutting and Grayson[24,25]. This surgery generates double-layered periosteal flaps and induces bone formation across the alveolar cleft without needing a donor site or graft[26].

Regarding the treatment outcome of GPP in unilateral CLP at 5 to 7 years of age, three-dimensional evaluation using cone-beam computed tomography (CT) showed that although a bone bridge was formed in the alveolar cleft region, the average height of the bone bridge was 44.4% of the total alveolar height[27]. It was reported that 41% of GPP-performed unilateral CLP cases required SBG afterwards[28]. A similar insufficient treatment outcome of GPP was reported in other studies for unilateral and bilateral CLP[29,30]. In cases with SBG, a sufficient bone bridge height was observed only in 45.8% of unilateral and bilateral CLP cases at 6 to 12 months after the operation[31]. Furthermore, it is reported that the mean bony bridge formation rate was 55.3% at 1 year of unilateral CLP cases after SBG[32]. A similar treatment outcome of SBG was reported in other studies for unilateral and bilateral CLP cases[33,34].

Based on the insufficient postsurgical outcome, regenerative medicine is expected to improve bone bridge formation and increase bone tissue formation in the alveolar cleft for CLP patients. In the field of regenerative medicine, stem cell transplantation is considered to be a powerful method. Mesenchymal stem cells (MSCs) have been isolated from various tissues such as the bone marrow, adipose tissue, and periodontal tissue[35–38]. However, bone marrow aspirates from the iliac bone and sternum are invasive and require large burden to the patients[35,39–41]. A recent study has shown that MSCs can be isolated from the umbilical cord, and isolated cells are known to be undifferentiated and have multipotency[42]. The collection and isolation of MSCs from umbilical cords are noninvasive to both mothers and infants. Moreover, human umbilical cord mesenchymal stem cells (hUCMSCs) have low immunogenicity, which is a great advantage in cases of allograft[43,44].

Previous *in vivo* studies have reported that CD146, a marker of MSCs, is related to high colony-forming, multipotency, and hematopoiesis-supporting abilities, and CD146-positive hUCMSCs are known to have a high differentiation potential to the osteogenic lineage[45]. In this study, we transplanted hUCMSCs into a rat alveolar cleft model and examined the osteogenic capacity, *in vivo*.

Materials and Methods

Cell Culture

Human umbilical cords were collected from five healthy full-term pregnant women aged 25 to 38 years who had undergone cesarean section at a maternity clinic after obtaining consent to umbilical cord collection. A 5- to 6-cm segment from the collected umbilical cord was cut into pieces of approximately 2 to 3 mm square using a sterile razor (Feather Safety Razor Co., Ltd., Osaka, Japan). Human umbilical cord stromal cells were isolated by enzymatic digestion (EZ method). Magnetic-activated cell sorting (MACS method) was used to enrich CD146-positive cells from cells isolated by the EZ method.

The EZ method was performed as described previously[46–48]. Briefly, the cut tissue pieces were transferred to 35 ml of a mixed solution (pH 7.4) of 3 mg/ml of collagenase type I (Merck KGaA, Darmstadt, Germany) and 4 mg/ml of dispase (Wako Pure Chemical Industries, Osaka, Japan) dissolved in Hanks' solution (Nissui Pharmaceutical Co., Ltd., Tokyo, Japan). After incubation at 37°C for 16 h, the mixture was subjected to separation of the cell components using a centrifuge (430 × g; KUBOTA 5800; Kubota Corporation Co., Ltd., Tokyo, Japan). Next, the cells were isolated using a 70-μm cell strainer (Merck KGaA), and 1×10^6 cells were seeded and cultured in a 100-mm culture dish (Corning, Corning, NY, USA). The growth medium used was α- minimum essential medium (MEM; Thermo Fisher Scientific, Waltham, MA, USA) supplemented with 10% fetal bovine serum (FBS; Lot No: S13025S1780, Biowest, Nuaillé, France), 100 μM glutamate (GlutaMAX I; Thermo Fisher Scientific), 0.1% MEM containing nonessential amino acids (Thermo Fisher Scientific), 50 U/ml of penicillin, 50 μg/ml of streptomycin (Thermo Fisher Scientific), and 0.25 mg/ml of Fungizone (Thermo Fisher Scientific). The obtained cells were defined as UC-EZ cells.

The MACS method was performed as described by Aslan et al.[49]. Briefly, 1 to 2×10^7 UC-EZ cells (passage number = 1) were treated with an FcR blocking reagent (Miltenyi Biotec, Bergisch Gladbach, Germany) for 10 min on ice to block nonspecific antibody binding. After the cells were mixed with CD146 microbeads at 4°C for 15 min, the mixture was washed with phosphate-buffered saline (PBS; Takara Bio, Kusatsu, Japan) (pH 7.4) containing 0.5% bovine serum albumin. After injecting 3 ml of PBS into an LS column (Miltenyi Biotec) in a MACS separator (Miltenyi Biotec), pelleted cells were resuspended in 500 μl of the same PBS solution and loaded onto the column. The flow-through fraction containing CD146-negative cells was discarded; the CD146-positive cells remaining in the column were eluted using a plunger and were collected in a 15-ml tube (Star; Rikaken Co., Ltd., Nagoya, Japan). The collected CD146-positive cells were defined as UC-MACS cells (passage number = 2).

UC-EZ cells were cultured at 37°C in a humidified atmosphere containing 5.0% CO_2. The growth medium was

Table 1. Primer Sequences for RT-PCR Analysis.

Genes		Primer sequence (5′→3′)	Product size (bp)	Accession number
NANOG	Forward	CAGAAGGCCTCAGCACCTAC	111	NM_024865.3
	Reverse	ATTGTTCCAGGTCTGGTTGC		
SOX2	Forward	AACCCCAAGATGCACAACTC	152	NM_003106
	Reverse	CGGGGCCGGTATTTATAATC		
OCT3/4	Forward	AACCCAGAACTTAGCAGCTT	861	NM_001173531
	Reverse	ACCTTCCCAAATAGAACCCCC		
GAPDH	Forward	GTCAAGGCTGAGAACGGGAA	613	NM_001289746.1
	Reverse	GCTTCACCACCTTCTTGATG		

GAPDH: gene encoding glyceraldehyde-3-phosphate dehydrogenase; RT-PCR: reverse transcription polymerase chain reaction.

replaced with fresh medium once every 3 days. After 70% to 80% confluency was reached, the cells were collected using TrypLE Select (1×) (Thermo Fisher Scientific) (hereafter, trypsin/ethylenediamine tetraacetic acid [EDTA]) and were subcultured at a ratio of 1:3; the cells with a passage from 2 to 4 were used for experiments. Isolated UC-MACS cells were used for experiments after being subcultured (passage number = 2 or 3). In subsequent experiments, cells from at least five different patients were used.

Flow Cytometry

UC-EZ and UC-MACS cells with a passage number of 3 were collected from culture dishes using trypsin/EDTA ($n = 5$), centrifuged for 5 min ($430 \times g$), and fixed with 4% paraformaldehyde (PFA) solution for 15 min. After adding various antihuman antibodies, the cells were incubated at room temperature for 1 h. According to the method described by Baksh et al.[50], the cells were incubated with the following primary antibodies on ice for 30 min in the dark: fluorescein isothiocyanate (FITC)-labeled mouse monoclonal antihuman CD14, CD45, CD73, CD105, and CD146 antibodies, phycoerythrin-labeled mouse monoclonal antihuman CD90 antibody (Becton Dickinson, Franklin Lakes, NJ, USA), FITC-labeled mouse monoclonal antihuman CD34 and CD44 antibodies (Beckman Coulter, Brea, CA, USA), and FITC-labeled mouse monoclonal antihuman CD19 (BioLegend, San Diego, CA, USA). The cells incubated with PBS alone without primary antibodies were used as negative controls. The cells incubated with the antibodies were washed with PBS, and then were subjected to a flow cytometer (SH800; Sony, Tokyo, Japan) to perform marker analysis of cell surface antigens of the primary antibodies used. Independent experiments were repeated three times for each antibody.

Reverse Transcription-Polymerase Chain Reaction

The RNeasy Mini Kit (Qiagen, Hilden, Germany) was used to extract total RNA from two cell types ($n = 5$) cultured to confluency. From 1 µg of prepared total RNA, cDNA was synthesized using the High Capacity cDNA Synthesis Kit (Thermo Fisher Scientific), and 20 µl of the reaction solution was prepared using Quick Taq HS DyeMix (Toyobo, Osaka, Japan). Polymerase chain reaction (PCR) was carried out using a 2720 Thermal Cycler (Thermo Fisher Scientific) as follows: 94°C for 2 min, followed by 35 cycles of 94°C for 30 s, 55°C for 30 s, and 72°C for 1 min. The primer sequences are shown in Table 1. Glyceraldehyde-3-phosphate dehydrogenase was used as an internal control. The PCR product solutions were electrophoresed on a 1.8% agarose gel containing 0.5 µg/ml of ethidium bromide, and the gel was observed under ultraviolet irradiation.

Multipotency Evaluation

Osteogenic differentiation. According to previous reports[51,52], two cell types were seeded at 2×10^4 cells/well in a 24-well plate and were cultured in the growth medium ($n = 5$). After confluency was reached, α-MEM (Thermo Fisher Scientific) supplemented with 10% FBS, 10 nM dexamethasone (Merck KGaA), 10 mM β-glycerophosphate (Merck KGaA), and 100 µM L-ascorbate-2-phosphate (Wako Pure Chemical) was used as the osteoblast differentiation induction medium. As negative controls, the cells were cultured similarly in α-MEM medium containing 10% FBS. The medium was changed every 3 days, and the cells were cultured for 3 weeks after the medium was changed to the induction medium.

Alizarin Red S staining was performed 3 weeks after culture in the induction medium to evaluate mineralized nodule formation. After removing the medium from each well, the cells were washed once with PBS and then fixed with 10% neutral buffered formalin (Wako Pure Chemical) for 10 min. The cells were strained with 1% Alizarin Red S (Merck KGaA) at room temperature for 30 min.

To examine immunostaining of osteopontin (OPN) in UC-MACS cells, cultured cells were also plated at 1×10^5 cells/well in four-well chamber slides and fixed with cold methanol for 10 min at −30°C. After washing with PBS, cells were incubated in Blocking One Histo (Nacalai Tesque, Kyoto, Japan) for 10 min at room temperature. Cultures were incubated with the rabbit polyclonal anti-OPN antibody (ab8448; Abcam, Cambridge, UK; dilution ratio 1:1,000) at 4°C overnight. After washing with PBS, the samples were incubated with the secondary antibody (Alexa Fluor 488-conjugated goat anti-rabbit IgG [Thermo

Fisher Scientific; dilution ratio 1:1,000]) for 30 min at room temperature in the dark. The samples were washed with PBS twice for 5 min each and mounted with fluoroshield mounting medium with DAPI (Funakoshi, Tokyo, Japan). Images were obtained by using a confocal laser-scanning microscope (LSM-800; Carl Zeiss, Oberkochen, Germany).

Chondrogenic differentiation. Cells were subjected to pellet culture as previously described[38] with minor modifications. Briefly, 1×10^6 cells in the growth medium were suspended in a 15-ml centrifuge tube (Becton Dickinson) and centrifuged at $430 \times g$ for 5 min to generate a pellet. Next, 1 ml of chondrogenic medium consisting of Dulbecco's modified Eagle medium/F12 containing 10% FBS, 10 ng/ml transforming growth factor-β1 (Peprotech, Oak Park, CA, USA), 1% ITS + 1 supplement (Merck KGaA), and 50 mM L-ascorbate-2-phosphate (Wako Pure Chemical) was gently added into the centrifuge tube. The differentiation medium was changed every 3 to 4 days during 4 weeks of differentiation cultivation, after which the pellets were fixed in 4% PFA, embedded in paraffin, and cut into 5 μm sections for histological analysis. Chondrogenic differentiation was determined by staining with 1% Alcian blue (Merck KGaA) solutions.

Adipogenic differentiation. According to the previous reports[53,54], two cell types were seeded at 2×10^4 cells/well in a 24-well plate and were cultured in growth medium ($n = 5$). After confluency was reached, α-MEM supplemented with 10% FBS, 0.5 mM 3-isobutyl-l-methylxanthine (Merck KGaA), 0.5 μM hydrocortisone (Wako Pure Chemical), and 60 μM indomethacin (Merck KGaA) was used as the adipocyte differentiation induction medium. As negative controls, the cells were cultured similarly in α-MEM medium containing 10% FBS. The medium was changed every 3 days, and the cells were cultured for 3 weeks after the medium was changed to the induction medium. Oil Red O staining was performed at 3 weeks after culture in the induction medium to evaluate the intracellular lipid droplets formed. After removing the medium from each well, the cells were washed twice with PBS and then fixed with 10% neutral buffered formalin for 15 min. After washing once with 60% isopropanol (Wako Pure Chemical), the wells were allowed to dry completely. The cells were stained with 0.2% Oil Red O solution (Wako Pure Chemical) at room temperature for 15 min. After washing each well four times with purified water, the lipid droplets formed were observed.

Evaluation of Bone Tissue Formation After Transplantation

In vivo transplantation. The composition of the scaffold (ReFit; HOYA, Tokyo, Japan) used for transplantation was HA: Col = 80:20, which is similar to that of actual bone tissue[55].

For general anesthesia, Sprague-Dawley rats (16-week-old males; CLEA Japan, Tokyo, Japan) received an intraperitoneal injection of the combination of three anesthetics: medetomidine hydrochloride (0.15 mg/kg: Meiji Pharmaceutical, Namerikawa, Japan), midazolam (2.0 mg/kg: Fuji Pharma, Tokyo, Japan), and butorphanol tartrate (2.5 mg/kg: Meiji Pharmaceutical). For local anesthesia, 1% lidocaine (1.5 mg/kg) (Showa Yakuhin Kako, Tokyo, Japan) was applied to the submucosal layer of the maxilla. After a longitudinal incision was made using a scalpel at the boundary between the maxilla and the alveolar mucosa, the alveolar mucosa was detached from the zygomatic arch to the ipsilateral maxillary incisor of the same side, and the periosteum was exposed. Next, a $5 \times 2.5 \times 1$ mm^3 bone defect was created in the maxilla using a manual low-speed drill as described previously[56,57]. The rats underwent transplantation of the scaffold only (HA + Col group), UC-MACS cells with the scaffold (HA + Col + UC-MACS group), or neither (negative control group) ($n = 5$ per group). In the first two groups, the scaffold in the same size as the bone defect was transplanted; in the HA + Col + UC-MACS group, 1×10^6 UC-MACS cells were seeded on the scaffold at the day before transplantation and were cultured overnight. After transplantation, the gingival mucosa was sutured using nonabsorbable sutures, and we confirmed that the animals came out from anesthesia. No immunosuppressants were used following the previous reports[43,58] describing the immunomodulatory effect of hUCMSCs.

Micro CT evaluation. Eight weeks after transplantation, the rats were euthanized by intraperitoneal injection of pentobarbital (70 mg/kg; Somnopentyl; Kyoritsu Seiyaku, Tokyo, Japan) (70 mg/kg). The maxilla was removed from each rat and was fixed with 4% PFA at 4°C for 3 days; 4% PFA was then substituted with 70% ethanol. Micro CT (μCT) images were taken with a CosmoScan GXII (90 kV, 88 μA, 50 voxels; Rigaku, Tokyo, Japan) ($n = 5$ per group).

Histological and immunohistochemical examination. The harvested maxilla was fixed in a 4% PFA solution, decalcified, and embedded in paraffin, and 4-μm-thick sections were prepared. Deparaffinized sections were stained with hematoxylin–eosin.

To quantitate the new bone formation in sections, the area of newly formed bone (BA) was calculated in bone defects using image analysis software (DP2-BSW; Olympus Life Science, Tokyo, Japan) ($n = 5$ for all three groups). BA was measured in the frontal section dissected at one-third of the total bone defects from the anterior end in each animal. The bone tissue rate (%) was calculated as BA (mm^2)/total tissue (mm^2) in each bone defect.

The primary antibodies used for immunohistochemical staining were rabbit antihuman OPN polyclonal antibody (ab8448; Abcam; dilution ratio 1:200) and mouse antihuman mitochondria monoclonal antibody (MAB1273; Merck KGaA; dilution ratio 1:80). After endogenous peroxidases were inactivated with PeroxAbolish (Biocare Medical, Pacheco, CA, USA), 10 mM citric acid treatment (95°C, 30 min) was performed for antigen activation depending
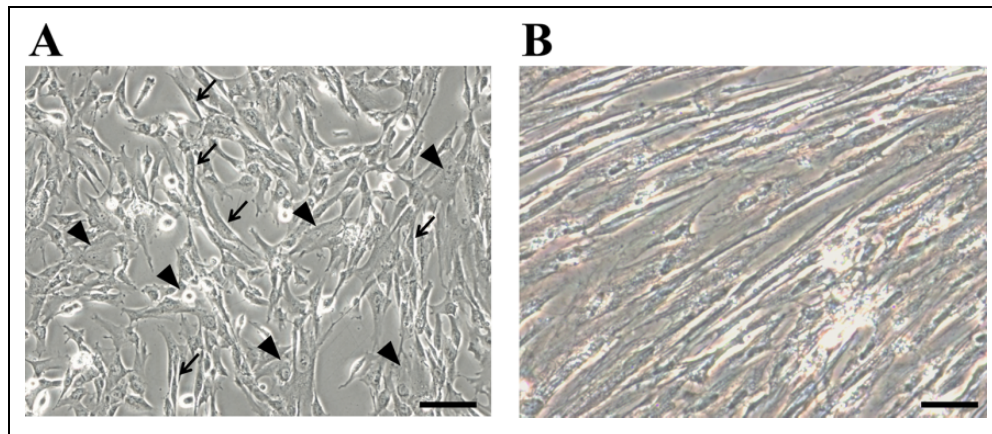
Fig. 1. Appearance of UC-EZ and UC-MACS cells. (A) UC-EZ cells isolated from the umbilical cord by enzymatic digestion and cultured for 1 week (passage 1). Arrows and arrowheads indicate spindle- and flat-shaped cells, respectively. (B) UC-MACS cells cultured for 1 week with a spindle cell appearance (passage 2). The appearance of the cultured cells was similar in five different cell preparations. Scale bars = 200 μm. UC-EZ cells were obtained from UC by EZ method. UC-MACS cells were extracted from UC-EZ by MACS method.

on the primary antibody used. Treatment with Blocking One Histo (Nacalai Tesque) at room temperature for 10 min was used to block nonspecific antibody binding. The primary antibodies described above were allowed to react overnight at 4°C. As the secondary Funa antibody, Dako Envision + Dual Link System-HRP (Dako, Glostrup, Denmark) was allowed to react at room temperature for 30 min. After color development with 3,3′-diaminobenzidine using the ImmPACT DAB Peroxidase Substrate Kit (Vector Laboratories, Burlingame, CA, USA), counterstaining was carried out with hematoxylin. As negative controls, the sections were stained according to the same procedure except that PBS was used instead of the primary antibodies.

Statistical Analysis

Statistical analysis was performed using IBM SPSS Statistics software (version 23.0; IBM Japan, Tokyo, Japan). One-way analysis of variance was employed for multiple comparisons of the bone tissue rate (%) among the three groups, followed by Tukey's post hoc methods. $P < 0.05$ was considered statistically significant.

This study was conducted using umbilical cords donated with approval from the Ethics Committees of Meikai University School of Dentistry (A1603) and Aiwa Hospital (maternity clinic). Animal experiments were planned in accordance with the rules of the Animal Experiment Ethics Committee of Meikai University School of Dentistry and were conducted after they were approved by the Laboratory Animals Ethics Committee (A1833).

Results

Cell Morphology

After culture for 4 days, cell populations with various morphologies, including spindle and flat-shaped cells, were observed in UC-EZ cells (Fig. 1A). By enriching CD146-positive cells, spindle-shaped cells were dominated in the culture of UC-MACS cells (Fig. 1B).

Cell Surface Marker Expression

The expressed surface antigens were analyzed by flow cytometry. In both cell types, CD14 (monocyte marker), CD19 (B cell marker), CD34 (hematopoietic stem cell marker), and CD45 (leukocyte antigen marker) were expressed only in a small proportion of cells ($\leq 7\%$).

In contrast, all MSC markers, CD44, CD73, CD90, and CD105, were expressed in more than 80% of UC-EZ cells. However, CD146 (pericyte marker and MSC marker) was only expressed in 48.8% of UC-EZ cells. CD44-, CD73-, and CD90-positive cells were more than 99.9%, and 86.5% were CD146 positive in US-MACS cells (Fig. 2).

Gene Expression Analysis by Reverse Transcription PCR

UC-EZ and UC-MACS cells were cultured in the growth medium until they reached confluency. Reverse transcription PCR analysis revealed that UC-EZ cells expressed *Nanog* and *Oct3/4* but not *Sox2*, which are genes related to the maintenance of the undifferentiated state. UC-MACS cells expressed *Nanog*, *Oct3/4*, and *Sox2* (Fig. 3). Furthermore, the expression of *Nanog* and *Oct3/4* in UC-MACS cells was higher than that in UC-EZ cells.

Osteogenic, Chondrogenic, and Adipogenic Differentiation of Cultured UC-EZ and UC-MACS Cells

To evaluate osteogenic differentiation, the formation of Alizarin Red-positive mineralized nodule was examined in UC-EZ and UC-MACS cells after 3 weeks of induction.
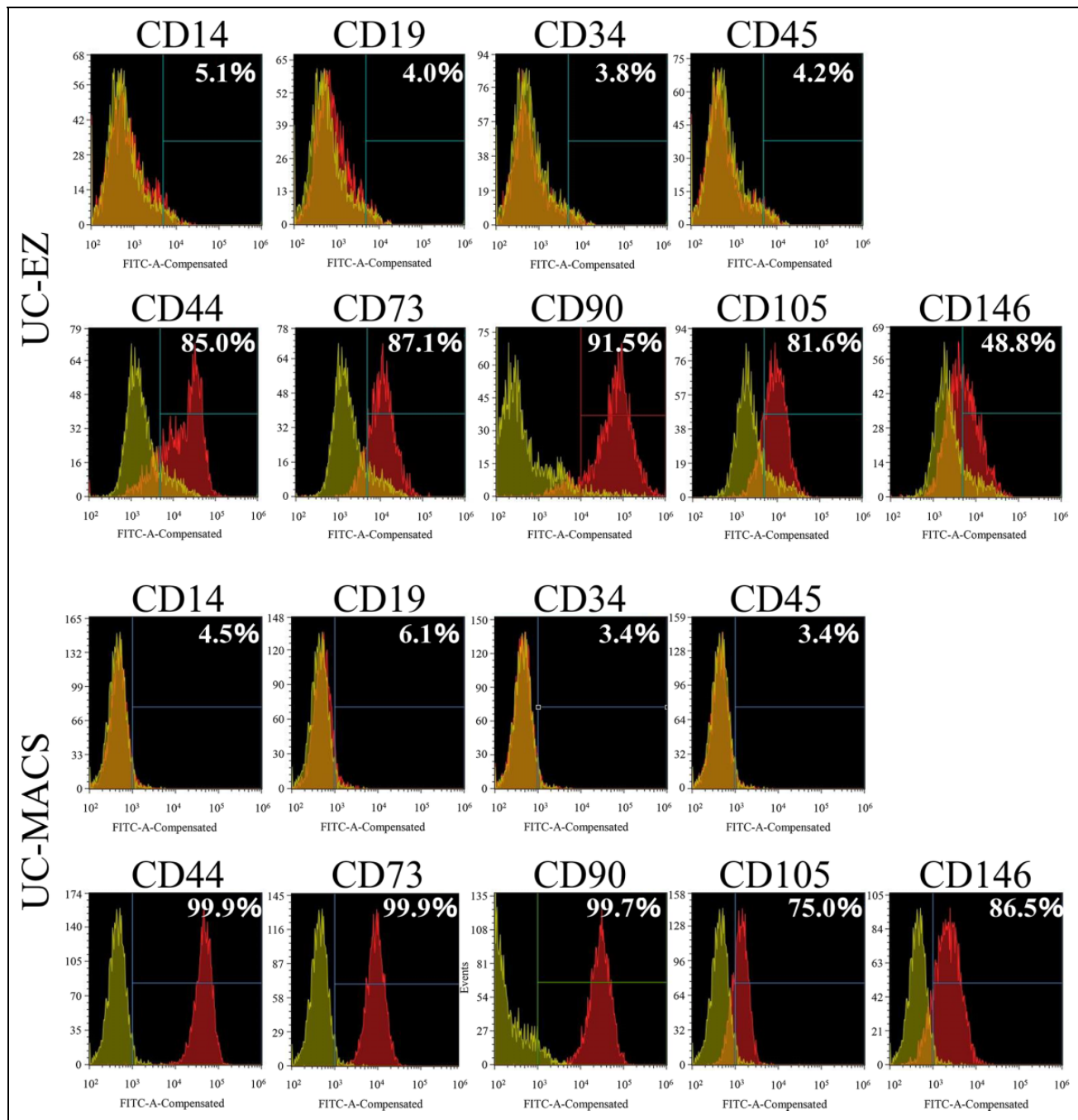
Fig. 2. Flow cytometric analysis of cell surface antigen expression in UC-EZ and UC-MACS cells. Expression of CD14, CD19, CD34, CD45, CD44, CD73, CD90, CD105, and CD146 in UC-EZ and UC-MACS cells. UC-EZ and UC-MACS cells were negative for CD14, CD19, CD34, and CD45 expression and positive for CD44, CD73, CD90, CD105, and CD146 expression. Similar results were obtained in five different cultures ($n = 5$). FITC: fluorescein isothiocyanate; UC-EZ: UC-MACS.

Many nodules were seen in both cell types cultured in the osteogenic induction medium (Fig. 4B, F). No mineralized nodule was formed in the cultures of the growth medium (Fig. 4A, E). No difference was found in the formation of mineralized nodules between the two cell types. To examine the osteogenic differentiation of UC-MACS cells further, immunohistochemical localization of OPN was examined

(Fig. 4F). Immunolocalization of OPN was seen in the cytoplasms of UC-MACS cells cultured under the osteogenic induction medium.

To evaluate chondrogenic differentiation, the pellet culture of UC-EZ and UC-MACS cells was performed for 4 weeks. After the culture period, alcian blue-stained sphere pellets were formed from both cells (Fig. 4C, G). However,
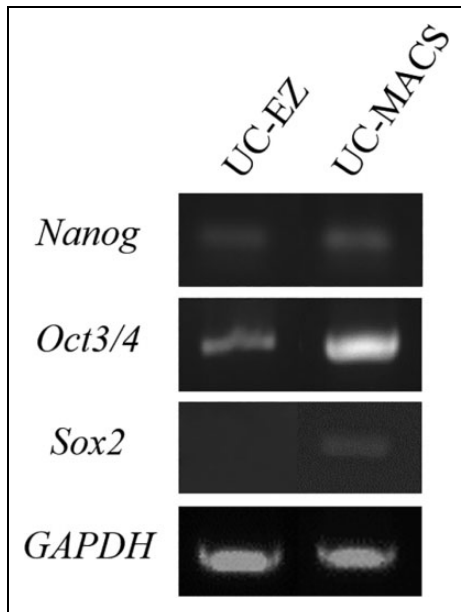
Fig. 3. Expression of pluripotent stem cell markers in UC-EZ and UC-MACS cells. Marker genes for pluripotent stem cells (*Nanog*, *Oct3/4*, and *Sox2*) were examined by reverse transcription polymerase chain reaction before the induction of cell differentiation. Both cell populations expressed *Nanog* and *Oct3/4*. The expression of *Sox2* was observed in UC-MACS cells but negligible in UC-EZ cells. Similar results were obtained from five different cultures. *GAPDH*: gene encoding glyceraldehyde-3- phosphate dehydrogenase; UC-EZ: UC-MACS.

the sphere formation, one of the features of chondrogenic differentiation[36,46], was insufficient by UC-EZ cells.

To evaluate adipogenic differentiation, the formation of Oil Red O-positive lipid droplets was examined in UC-EZ and UC-MACS cells after 3 weeks of induction. Many lipid droplets were observed in both cell types cultured in the adipogenic induction medium (Fig. 4D, H). No lipid droplet was formed in the cultures of the growth medium (data not shown). No difference was observed in the formation of lipid droplets between the two cell types.

In Vivo Osteogenesis

μ*CT examination.* μCT images were acquired immediately after the bone defect was generated in the rat maxillae (Fig. 5A–F). The CT values were markedly low in the regions of the bone defect with clear bounding (Fig. 5A–C). Immediately after the scaffold was transplanted into the defect, the scaffold was visible and distinguishable from the bone by a dot-like appearance (Fig. 5D–F).

The purpose of this study was to clarify the bone formation activity of hUCMSCs. In the following *in vivo* experiments, we took advantage of using UC-MACS cells including higher ratio of hUCMSCs (Figs. 2 and 3). Eight weeks after transplantation, the negative control group showed no bone bridge formation in the bone defect with a

small number of island-shaped opacities (Fig. 5G-I). In the HA + Col group, a thin bone bridge was observed between the bone defect (Fig. 5J-L). In the HA + Col + UC-MACS group, a bone bridge was formed between the defect and the dot-like appearance showed a much higher CT value than that at immediately after transplantation (Fig. 5M-O). Similar results were obtained from each group (*n* = 5).

Histological examination. Hematoxylin–eosin-stained sections in the negative control group revealed no bone bridge formation and a few island-shaped new bones were seen in the bone defect region at 8 weeks after operation (Fig. 6A, B). In the HA + Col group, thin bone tissue was formed between the bone defect. Many scaffolds (HA + Col) were unresorbed and remained in the new bone (Fig. 6C, D). In the HA + Col + UC-MACS group, a wide bone tissue was formed between the bone defect. The scaffolds were also found to be unresorbed in this group (Fig. 6E, F). The border between the pre-existing bone and newly formed bone was distinguishable in each group (insert in Fig. 6B). In quantitative analysis of the bone tissue rate (%), the values for the HA + Col group (44.0% ± 5.7%) and HA + Col + UC-MACS group (60.5% ± 6.9%) were significantly higher than those of the negative control group (24.5% ± 7.6%) (Fig. 6G). The bone tissue rate (%) of the HA + Col + UC-MACS group was also significantly higher than that of the HA + Col group.

Immunohistochemical examination. OPN-positive cells were observed on the surface of new bones in the negative control group at 8 weeks after operation (Fig. 7A, B). In the HA + Col-only transplanted group and HA + Col + UC-MACS-transplanted group, OPN-positive cells were seen along the newly formed bone surface and were also embedded in the new bone at 8 weeks after transplantation (Fig. 7C-F).

To highlight the localization of transplanted UC-MACS cells in the bone defects, the immunological reaction to an anti-human-specific mitochondria antibody was examined. Human-specific mitochondria-positive cells were aligned along the newly formed bone surface and in the nonmineralized tissue at 4 and 8 weeks after transplantation in the HA + Col + UC-MACS-transplanted group (Fig. 7G, H, J, K). Positive cells were embedded in the new bone (Fig. 7 J-L) at 8 weeks but not at 4 weeks after transplantation (Fig. 7G, H). No positive cells were found in the HA + Col-only transplanted group (Fig. 7I).

Discussion

CLP causes several morphological and functional abnormalities in maxillofacial regions, even after the surgical closure of the lip and palate[7–12]. Insufficient bony support at the base of the nasal wing causes asymmetry of the base of the nasal wing[59]. Naso-oral fistulas cause speech problems, retention of food, and reflux of nasal discharge[60]. In addition to esthetic problems, alveolar cleft causes limitations in
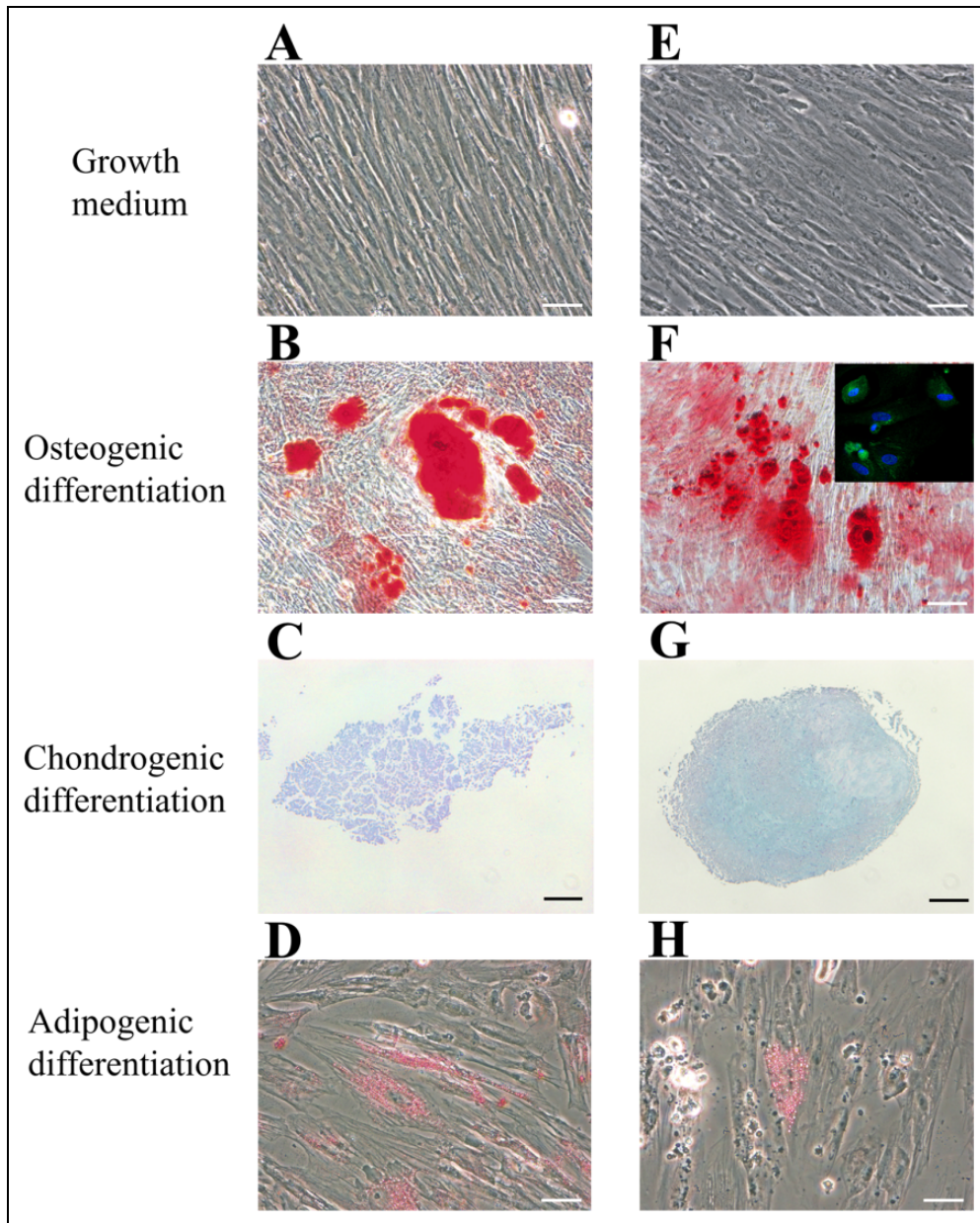
Fig. 4. *In vitro* differentiation of UC-EZ and UC-MACS cells. UC-EZ (B) and UC-MACS (F) cells were cultured in the osteogenic induction medium for 3 weeks. (B, F) Alizarin red S staining showed the mineralized nodules in the cultures of UC-EZ and UC-MACS cells, respectively. Insert in F: Immunolocalization of osteopontin (green) in UC-MACS cells cultured in the osteogenic induction medium for 3 weeks. Nuclei were stained with DAPI (blue). (A, E) No mineralized nodule formation was observed, when both cell types were cultured in the growth medium and stained. Scale bars = 100 μm. UC-EZ (C) and UC-MACS (G) cells were subjected to pellet culture in the chondrogenic induction medium for 4 weeks. After the culture, pellets were fixed, embedded in paraffin, and stained with alcian blue solution. (C, G) scale bars = 200 μm. UC-EZ (D) and UC-MACS (H) cells were cultured in the adipogenic induction medium for 3 weeks. (D, H) Oil red O staining showed the lipid clusters in the cultures of UC-EZ and UC-MACS cells, respectively. Scale bars = 100 μm. UC-EZ: UC-MACS.

orthodontic tooth movement and worsens the outcome of prosthetic treatment[61]. Therefore, surgical closure by GPP and SBG is important to obtain normal function and acceptable appearance. To improve the treatment outcome of these surgeries, hUCMSCs were examined in the experimental model of alveolar clefts.

In the regenerative medicine, one of the great advantages of using hUCMSCs is that these cells retain low immunogenicity and have an immunomodulatory effect[62,63]. hUCMSCs cannot induce allogeneic peripheral blood mononuclear cell (PBMC) proliferation and inhibit the immune responses of PBMCs, *in vitro*[63]. It was also reported that
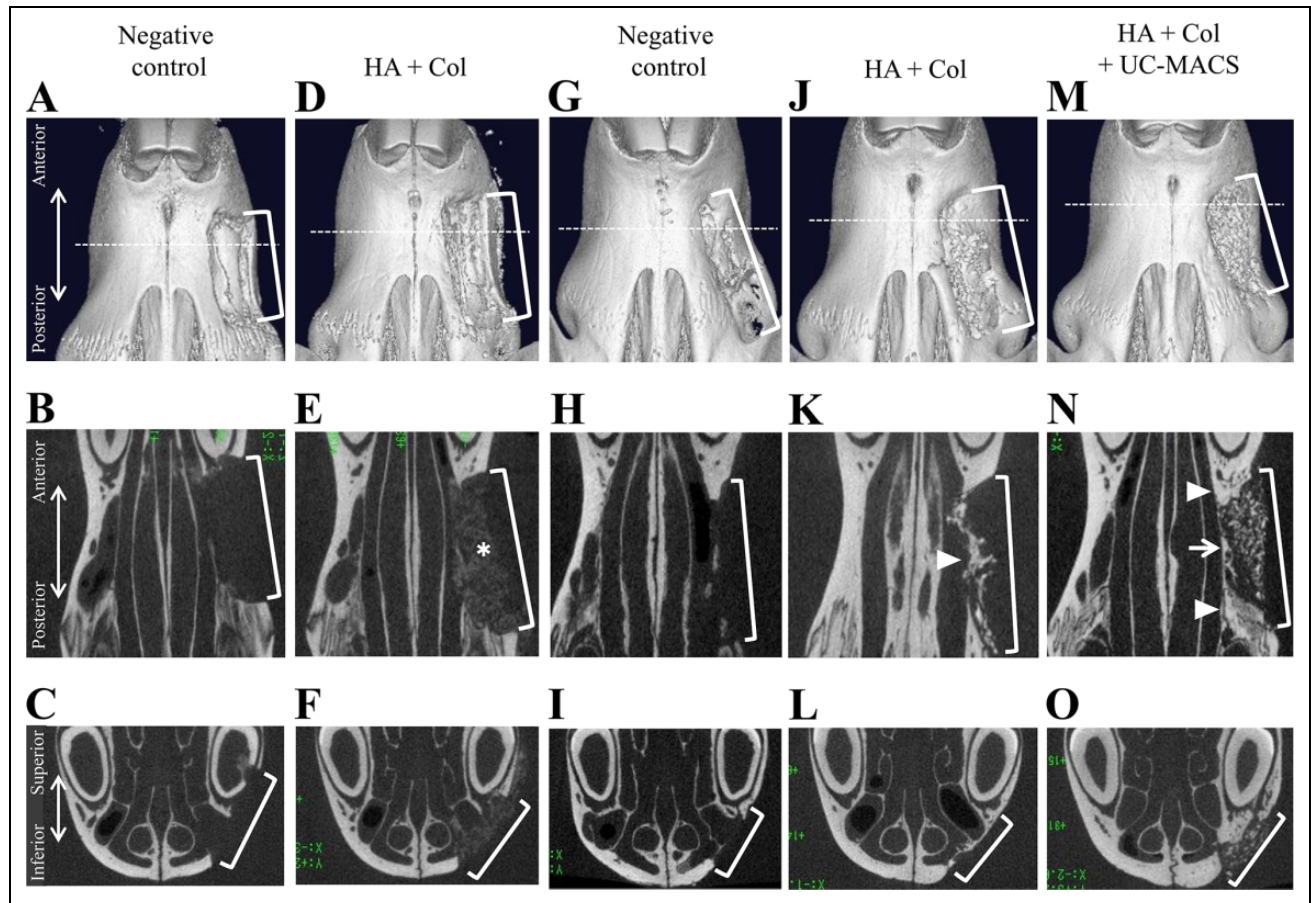
Fig. 5. μCT images of the 16-week-old rat maxillary defects immediately and at 8 weeks after operation. (A-F) Representative μCT images immediately after operation. (G-O) Representative μCT images at 8 weeks after operation. Ventral view of 3D reconstructed maxillae (A, D, G, J, M), horizontal cross-sections (B, E, H, K, N), and coronal cross-sections (C, F, I, L, O) showing maxillary bone defects. Dotted lines of 3D images denote the position at one-third of the total bone defects from the anterior end (A, D, G, J, M). Frontal views in C, F, I, L, and O were sliced at the white dotted lines in A, D, G, J, and M, respectively. Bone defects of the negative control (A-C, G-I), transplanted scaffold (HA + Col) only (D-F and J-L), and transplanted scaffold (HA + Col) with UC-MACS cells (M-O). Since the border of each defect was clearly distinguished from the undissected bone, the defected areas are highlighted by white solid lines in A-O. The asterisk in E indicates the scaffold (HA + Col). Arrowheads in K and N indicate new bone formation with high CT value. Similar observations were noted in five different experiments ($n = 5$). Col: collagen; HA: hydroxyapatite; μCT: micro computed tomography; 3D: three-dimensional; UC-MACS.

hUCMSCs did not express CD40, CD40 ligand, CD80, CD86, and major histocompatibility complex class II molecules, all of which are essential factors in the normal immune system[63].

In this study, CD146 (also known as MCAM, Mel-CAM, S-Endo-1, A32 antigen, and MUC18) was used to select UC-MACS cells. CD146 is expressed on several cell types (e.g., MSCs, endothelial cells, and melanoma cells) and related to heterotypic intercellular adhesion[64,65]. CD146 was identified as an early mesenchymal marker present in MSCs derived from human bone marrow, dental pulp, adipose tissues, and the umbilical cord[45,66–68]. High proliferative potential and multipotency were observed in CD146-positive cells[50,69]. In this study, we used MACS method to enrich CD146-positive cells. It is known that MACS is a simple and reliable procedure to enrich cells expressing specific cell markers[70]. MACS can sort cells with increased yield and reduced cellular stress compared with FACS[71]. Using MACS method, CD146-positive cells were increased from 48.8% to 86.5% in UC-MACS cells. As shown in Fig. 1, UC-EZ cells contained cells with various morphologies and UC-MACS cells comprised mainly by spindle-shaped cells. This finding is consistent with that in a previous study reporting that CD146-positive cells showed spindle shape and had fibroblastic phenotype[45,65,72].

Nanog, *Oct3/4*, and *Sox2* are transcription factors related to the maintenance of the multipotency of ES and iPS cells[73]. Expression of *Nanog* and *Oct3/4* but not *Sox2* was observed in UC-EZ cells (Fig. 3). This finding was consistent with that in a study reporting that UCMSCs expressed these stemness genes at lower level than those in ES and iPS cells[74]. Interestingly, all three genes were expressed in UC-MACS cells
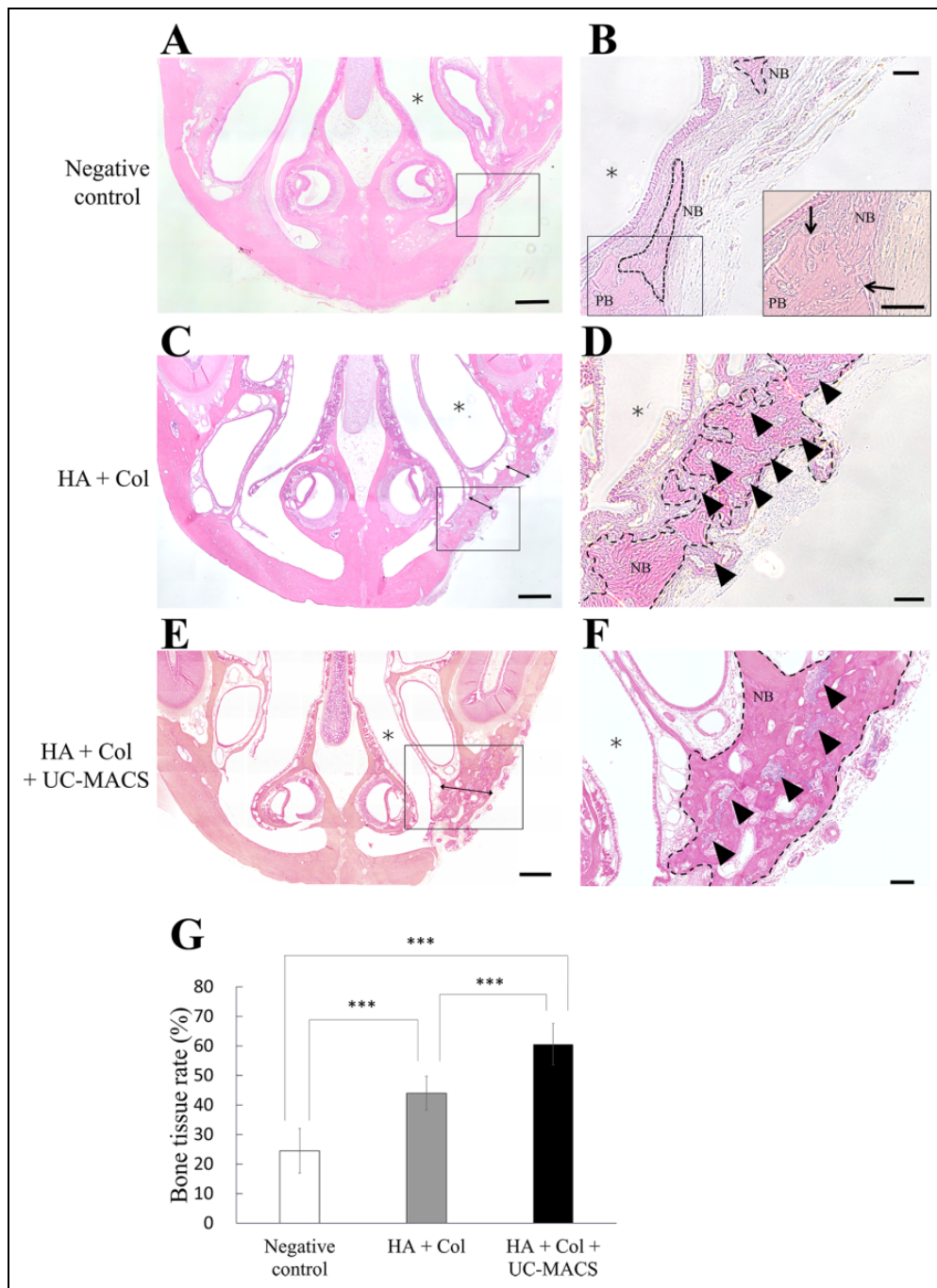
Fig. 6. Histological observation of the 16-week-old rat maxillary defects at 8 weeks after operation. Hematoxylin and eosin staining of negative control groups (A, B), scaffold (HA + Col)-only transplanted groups (C, D), and scaffold (HA + Col) with UC-MACS-transplanted groups (E, F). Boxed areas in A, C, and E are shown in higher magnification in B, D, and F, respectively. The boxed area in B is shown in higher magnification in the insert. The arrows in B denote the border of pre-existing bone and newly formed bone. Scaffolds (HA + Col) are shown by arrowheads in D and F. Asterisks indicate the nasal cavity (A, B, C, D, E). Scale bars = 1 mm; (B, D, F) Scale bars = 200 µm. The black dotted lines indicate the border of new bone with a woven appearance. A similar observation was noted in five different experiments ($n = 5$). Quantitative analysis of the bone tissue rate (%) in each group ($n = 5$) is shown in G. ***$P < 0.001$. Col: collagen; HA: hydroxyapatite; NB: new bone; PB: pre-existing bone; UC-MACS.
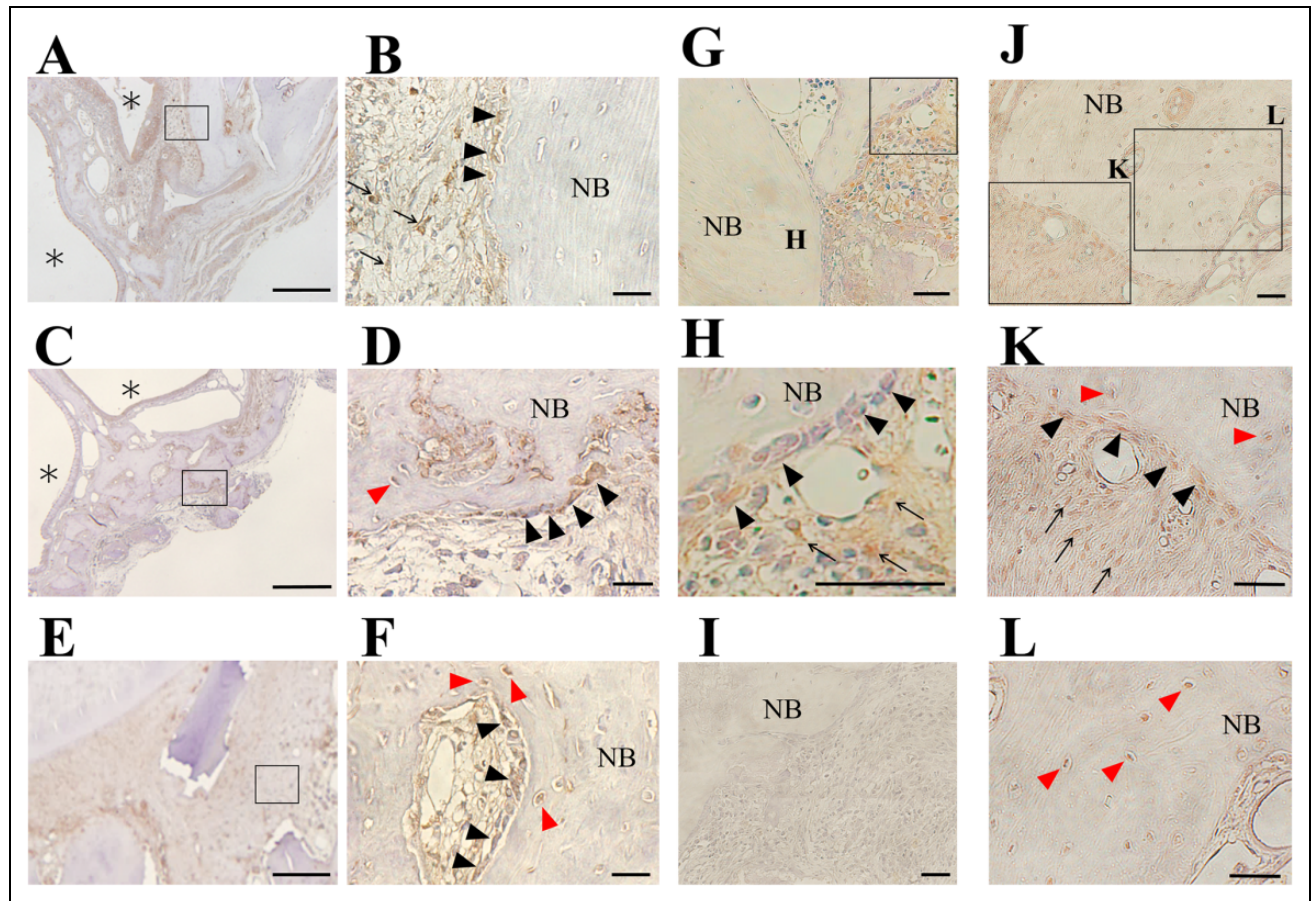
Fig. 7. Immunohistochemical staining of the 16-week-old rat alveolar bone defects at 4 and 8 weeks after operation. Immunohistochemical staining for OPN (A-F) at 8 weeks after operation. Negative control groups (A-B), scaffold (HA + Col)-only transplanted groups (C, D), and scaffold (HA + Col) with UC-MACS cells-transplanted groups (E, F). The boxed areas in A, C, and E are shown in higher magnification in B, D, and F, respectively. The black arrowheads in B, D, and F indicate OPN-positive cells along the newly formed bone surface. The red arrowheads in D and F indicate OPN-positive cells embedded in the newly formed bone. The arrows in B indicate OPN-positive cells in nonmineralized tissue. Immunohistochemical staining for human-specific mitochondria at 4 weeks (G-I) and 8 weeks (J-K) after transplantation. Scaffold (HA + Col)-only transplanted group (I), and scaffold (HA + Col) with UC-MACS cells-transplanted groups (G, H, J-L). The boxed area in G is shown in higher magnification in H. The boxed areas in J are shown in higher magnification in K and L. The black arrowheads and arrows in H and K indicate human-specific mitochondria-positive cells along the bone surface and in nonmineralized tissue, respectively. The red arrowheads in K and L indicate human-specific mitochondria-positive cells embedded in the bone tissue. No positive cells were seen in scaffold (HA + Col)-only transplanted group (I). (A, C, E) Scale bars = 500 μm. (B, D, F, G-L): Scale bars = 50 μm. The asterisks indicate the nasal cavity (A, C). Similar observations were noted in five different experiments ($n = 5$). Col: collagen; HA: hydroxyapatite; NB: new bone; OPN: osteopontin; UC-MACS.

(Fig. 3). It is reported that CD146-positive cells expressed higher levels of stemness genes than CD146-negative cells in hUCMSCs. Moreover, gene knockdown of CD146 in MSCs resulted in the decreased expression of stemness genes[75]. These studies and the result of UC-MACS cells suggest that expression of stemness genes is associated with CD146 expression.

In this study, 16-week-old rats were used to generate alveolar bone defects. To evaluate new bone formation of the craniofacial region *in vivo*, the calvarial defect model has been widely used[76,77]. In this model, 8- to 10-week-old rats have been mostly used. In the alveolar cleft model shown in Fig. 6G, spontaneous new bone formation was 24.5% ± 7.6%

in the negative control without any carrier or cells at 8 weeks after generating the alveolar defect. In the calvarial defect model, the new bone formation was only 11.0% ± 6.3% at 12 weeks after surgery under the same condition[78]. One of the reasons for the lower value in the calvarial defect model was that this model was less supplied with blood and nutrients to induce bone formation[79]. Alveolar cleft repair is reported to occur relatively fast[57], and it would be difficult to examine the precise effect of hUCMSCs on the bone formation in our experiment using animals younger than 16 weeks.

The critical size in the rat calvarial defect is known as 8 mm in diameter[80]. Using this calvarial model, many studies examined bone formation at 12 weeks after generating

the defect[78–80]. In this study, 8 weeks of bone formation was examined after the alveolar defect was generated in rats. The critical defect size of the alveolar defect model was reported as $5 \times 2.5 \times 1$ mm^3, as in this study[57,78]. Although the alveolar defect model had a three-dimensional structure, each side was smaller than that of the calvarial defect model. Thus, the alveolar bone defect is prone to be filled with the new bone in a shorter time than the calvarial defect.

The scaffold used in this study is porous and elastic under wet conditions[55]. As shown in Figs. 5 and 6, new bone formation was observed around the scaffold. The scaffold itself had low CT value before transplantation. This scaffold was reported to be absorbed and replaced by the new bone mostly by 8 weeks and almost completely by 12 weeks after transplantation in the tibial defect in rabbits[81]. These features are suitable as a bioresorbable carrier for bone formation.

Previous studies have shown that hUCMSCs are useful for bone regeneration[78,82–84]. Among them, it is reported that CD146-positive hUCMSCs showed osteogenic differentiation and new bone regeneration in femoral defect of SCID mice[45]. In this study and in other studies, CD146-positive cells have higher multipotency than CD146- negative cells[50,69]. Thus, UC-MACS cells were used and examined in the alveolar defect model. As shown in Figs. 5 and 6, UC-MACS cells, CD146-positive hUCMSCs, showed abundant new bone formation in the experimental alveolar clefts. The precise cellular mechanism regarding how UC-MACS cells could induce bone formation is unclear. However, human-specific mitochondria positive-cells were aligned along the newly formed bone surface at both 4 and 8 weeks after transplantation (Fig. 7 H, K). Positive cells were embedded in the new bone tissue like osteocytes at 8 weeks (Fig. 7 K, L) but not at 4 weeks (Fig. 7 H) after transplantation. Osteocytes are cells derived from osteoblasts, and trapped in the matrix that osteoblasts secrete[85]. These findings suggest that UC-MACS cells induced the new bone formation via osteoblastic differentiation in the present alveolar defect model.

Conclusion

The two types of hUCMSCs were obtained in this study. CD146-positive UC-MACS cells generated a sufficient bone bridge between the experimental alveolar clefts. These findings indicate that human umbilical cords are reliable bioresource and UC-MACS cells are useful for the alveolar cleft regeneration.

Ethical Approval

This study was conducted using donated umbilical cords after approval from the Ethics Committees of Meikai University School of Dentistry (approval number A1603) and Aiwa Hospital (maternity clinic).

Statement of Animal Rights

Animal experiments were planned in accordance with the rules of the Animal Experiment Ethics Committee of Meikai University School of Dentistry and conducted after they were approved by the Laboratory Animals Ethics Committee (approval number A1833).

Statement of Informed Consent

The patients provided written informed consent for their information and images to be published.

Declaration of Conflicting Interests

The author(s) declared no potential conflicts of interest with respect to the research, authorship, and/or publication of this article.

ORCID iD

Akiko Toyota https://orcid.org/0000-0002-8999-0607

References

1. Mossey PA, Little J, Munger RG, Dixon MJ, Shaw WC. Cleft lip and palate. Lancet. 2009;374(9703):1773–1785.
2. Dixon MJ, Marazita ML, Beaty TH, Murray JC. Cleft lip and palate: understanding genetic and environmental influences. Nat Rev Genet. 2011;12(13):167–178.
3. Raut JR, Simeone RM, Tinker SC, Canfield MA, Day RS, Agopian AJ. Proportion of orofacial clefts attributable to recognized risk factors. Cleft Palate Craniofac J. 2019; 56(12):151–158.
4. Mossey P. Epidemiology underpinning research in the aetiology of orofacial clefts. Orthod Craniofac Res. 2007;10(3): 114–120.
5. Toro-Ibacache V, Cortés Araya J, Díaz Muñoz A, Manríquez Soto G. Morphologic variability of nonsyndromic operated patients affected by cleft lip and palate a geometric morphometric study. Am J Orthod Dentofacial Orthop. 2014;146(3): 346–354.
6. Panamonta V, Pradubwong S, Panamonta M, Chowchuen B. Global birth prevalence of orofacial clefts: a systematic review. J Med Assoc Thai. 2015;98(Suppl 7):11–21.
7. Calzolari E, Pierini A, Astolfi G, Bianchi F, Neville AJ, Rivieri F.Associated anomalies in multi-malformed infants with cleft lip and palate: an epidemiologic study of nearly 6 million births

in 23 EUROCAT registries. Am J Med Genet A. 2007; 143A(6):528–537.

8. Kluba S, Bopp C, Bacher M, Reinert S, Krimmel M.Morphological analysis of the lip and nose following cleft lip repair with simultaneous partial primary rhinoplasty: a prospective study over 4 years. J Craniomaxillofac Surg. 2015;43(5): 599–605.

9. Sasaki R, Arakaki K, Tamura F, Kikutani T, Sunakawa H. Analysis of tongue movements during sucking by infants with cleft lip and palate using a diagnostic ultrasound device: changes during the six months after birth. J Oral Maxillofac Surg Med Pathol. 2014;26(4):456–463.

10. Paradowska-Stolarz A, Kawala B. Occlusal disorders among patients with total clefts of lip, alveolar bone, and palate. BioMed Res Int. 2014;2014:583416.

11. Kappen IFPM, Bittermann D, Janssen L, Bittermann GKP, Boonacker C, Haverkamp S, de Wilde H, van Der Heul M, Specken TF, Koole R, Kon M, et al.Long-term follow-up study of young adults treated for unilateral complete cleft lip, alveolus, and palate by a treatment protocol including two stage palatoplasty: speech outcomes. Arch Plast Surg. 2017;44(3): 202–209.

12. Kalaiarasi R, Syed KA, Vijayakumar C, Varghese AM, John M. Clinical study on middle ear diseases in children with orofacial clefts. Cureus. 2018;10(2):e2175.

13. Randall P. A triangular flap operation for the primary repair of unilateral clefts of the lip. Plast Reconstr Surg. 1959;23(3): 331–347.

14. Millard DR Jr. Rotation-advancement principle in cleft lip closure. Cleft Palate J. 1964;12:246–252.

15. Onizuka T. A new method for the primary repair of unilateral cleft lip. Ann Plast Surg. 1980;4(6):516–524.

16. Wardill WEM. The technique of operation for cleft palate. Br J Surg. 1937;25(97):117–130.

17. Furlow LT Jr. Cleft palate repair by double opposing Z-plasty. Plast Reconstr Surg. 1986;78(6):724–738.

18. Boyne PJ, Sands NR. Secondary bone grafting of residual alveolar and palatal clefts. J Oral Surg. 1972;30(2):87–92.

19. Boyne PJ, Sands NR. Combined orthodontic-surgical management of residual palato-alveolar cleft defects. Am J Orthod. 1976;70(1):20–37.

20. Bergland O, Semb G, Abyholm F, Borchgrevink H, Eskeland G. Secondary bone grafting and orthodontic treatment in patients with bilateral complete clefts of the lip and palate. Ann Plast Surg. 1986;17(16):460–474.

21. Long RE Jr, Spangler BE, Yow M. Cleft width and secondary alveolar bone graft success. Cleft Palate Craniofac J. 1995; 32(5):420–427.

22. Jia YL, James DR, Mars M. Bilateral alveolar bone grafting: a report of 55 consecutively-treated patients. Eur J Orthod. 1998; 20(3):299–307.

23. Rawashdeh MA, Al Nimri KS. Outcome of secondary alveolar bone grafting before and after eruption of the canine in Jordanian patients with cleft lip and palate. J Craniofac Surg. 2007; 18(6):1331–1337.

24. Skoog T.The use of periosteum and surgicel for bone restoration in congenital clefts of the maxilla. A clinical report and experimental investigation. Scand J Plast Reconstr Surg. 1967; 1(2):113–130.

25. Grayson BH, Cutting CB. Presurgical nasoalveolar orthopedic molding in primary correction of the nose, lip, and alveolus of infants born with unilateral and bilateral clefts. Cleft Palate Craniofac J. 2001;38(3):193–198.

26. Hoppper RA, Al-Mufarrej F. Gingivoperiosteoplasty. In: Losee JE, Kirschner RE, editors. Comprehensive Cleft Care. Boca Raton (FL): CRC Press; 2015. p. 1309–1320.

27. Mano M, Tokioka K, Matsumoto M, Tanaka E, Hasegawa H, Shinagawa R, Minoda A, Tomita S, Nakatsuka T, Suda N. Three-dimensional analysis of alveolar cleft after gingivoperiosteoplasty (GPP) in unilateral cleft lip and palate (UCLP) children. J Jpn Cleft Palate Assoc. 2014;39(3):201–208.

28. Matic DB, Power SM. Evaluating the success of gingivoperiosteoplasty versus secondary bone grafting in patients with unilateral clefts. Plast Reconstr Surg. 2008; 121(4):1343–1353.

29. Santiago PE, Grayson BH, Cutting CB, Gianoutsos MP, Brecht LE, Kwon SM. Reduced need for alveolar bone grafting by presurgical orthopedics and primary gingivoperiosteoplasty. Cleft Palate Craniofac J. 1998;35(1):77–80.

30. Sato Y, Grayson BH, Garfinkle JS, Barillas I, Maki K, Cutting CB. Success rate of gingivoperiosteoplasty with and without secondary bone grafts compared with secondary alveolar bone grafts alone. Plast Reconstr Surg. 2008;121(4):1356–1367.

31. Kawakami S, Hiura K, Sumitani K, Yokozeki M, Moriyama K. Prognosis of bone grafting into alveolar clefts with autogenous cancellous bone: a clinical evaluation using dental radiographs and computed tomographs. Orthodontic waves. 2000;59(1): 12–20.

32. Feng B, Jiang M, Xu X, Li J. A new method of volumetric assessment of alveolar bone grafting for cleft patients using cone beam computed tomography. Oral Surg Oral Med Oral Pathol Oral Radiol. 2017;124(2):171–182.

33. Tai CC, Sutherland IS, McFadden L. Prospective analysis of secondary alveolar bone grafting using computed tomography. J Oral Maxillofac Surg. 2000;58(11):1241–1249.

34. Feichtinger M, Zemann W, Mossböck R, Kärcher H. Three-dimensional evaluation of secondary alveolar bone grafting using a 3D- navigation system based on computed tomography: a two-year follow-up. Br J Oral Maxillofac Surg. 2008; 46(4):278–782.

35. Pittenger MF, Mackay AM, Beck SC, Jaiswal RK, Douglas R, Mosca JD, Moorman MA, Simonetti DW, Craig S, Marshak DR. Multilineage potential of adult human mesenchymal stem cells. Science. 1999;284(5411):143–147.

36. Kern S, Eichler H, Stoeve J, Klüter H, Bieback K. Comparative analysis of mesenchymal stem cells from bone marrow, umbilical cord blood, or adipose tissue. Stem Cells. 2006;24(5): 1294–1301.

37. Tamaki Y, Nakahara T, Ishikawa H, Sato S. In vitro analysis of mesenchymal stem cells derived from human teeth and bone marrow. Odontology. 2013;101(2):121–132.

38. Shinagawa-Ohama R, Mochizuki M, Tamaki Y, Suda N, Nakahara T. Heterogeneous human periodontal ligament-committed progenitor and stem cell populations exhibit a unique cementogenic property under *in vitro* and *in vivo* conditions. Stem Cells Dev. 2017;26(9):632–645.

39. Friedenstein AJ, Gorskaja JF, Kulagina NN. Fibroblast precursors in normal and irradiated mouse hematopoietic organs. Exp Hematol. 1976;4(5):267–274.

40. Bianco P, Gehron Robey P. Marrow stromal stem cells. J Clin Invest. 2000;105(12):1663–1668.

41. Caplan AI. Adult mesenchymal stem cells for tissue engineering versus regenerative medicine. J Cell Physiol. 2007;213(2):341–347.

42. Romanov YA, Svintsitskaya VA, Smirnov VN. Searching for alternative sources of postnatal human mesenchymal stem cells: candidate MSC-like cells from umbilical cord. Stem Cells. 2003;21(1):105–110.

43. Weiss ML, Anderson C, Medicetty S, Seshareddy KB, Weiss RJ, VanderWerff I, Troyer D, McIntosh KR. Immune properties of human umbilical cord Wharton's jelly-derived cells. Stem Cells. 2008;26(11):2865–2874.

44. Zhang J, La X, Fan L, Li P, Yu Y, Huang Y, Ding J, Xing Y. Immunosuppressive effects of mesenchymal stem cell transplantation in rat burn models. Int J Clin Exp Pathol. 2015; 8(5):5129–5136.

45. Tsang WP, Shu Y, Kwok PL, Zhang F, Lee KK, Tang MK, Li G, Chan KM, Chan WY, Wan C. CD146+ Human umbilical cord perivascular cells maintain stemness under hypoxia and as a cell source for skeletal regeneration. PLoS One. 2013;8(10): e76153.

46. Wang HS, Hung SC, Peng ST, Huang CC, Wei HM, Guo YJ, Fu YS, Lai MC, Chen CC. Mesenchymal stem cells in the Wharton's jelly of the human umbilical cord. Stem Cells. 2004;22(7):1330–1337.

47. Schugar RC, Chirieleison SM, Wescoe KE, Schmidt BT, Askew Y, Nance JJ, Evron JM, Peault B, Deasy BM. High harvest yield, high expansion, and phenotype stability of CD146 mesenchymal stromal cells from whole primitive human umbilical cord tissue. J Biomed Biotechnol. 2009; 2009:789526.

48. Can A, Balci D. Isolation, culture, and characterization of human umbilical cord stroma-derived mesenchymal stem cells. Methods Mol Biol. 2011;698:51–62.

49. Aslan H, Zilberman Y, Kandel L, Liebergall M, Oskouian RJ, Gazit D, Gazit Z. Osteogenic differentiation of noncultured immunoisolated bone marrow-derived CD105+ cells. Stem Cells. 2006;24(7):1728–1737.

50. Baksh D, Yao R, Tuan RS. Comparison of proliferative and multilineage differentiation potential of human mesenchymal stem cells derived from umbilical cord and bone marrow. Stem Cells. 2007;25(6):1384–1392.

51. Cheng H, Qiu L, Ma J, Zhang H, Cheng M, Li W, Zhao X, Liu K. Replicative senescence of human bone marrow and umbilical cord derived mesenchymal stem cells and their differentiation to adipocytes and osteoblasts. Mol Biol Rep. 2011; 38(8):5161–5168.

52. Wang KX, Xu LL, Rui YF, Huang S, Lin SE, Xiong JH, Li YH, Lee WY, Li G. The effects of secretion factors from umbilical cord derived mesenchymal stem cells on osteogenic differentiation of mesenchymal stem cells. PLoS One. 2015;10(3): e0120593.

53. Saben J, Thakali KM, Lindsey FE, Zhong Y, Badger TM, Andres A, Shankar K. Distinct adipogenic differentiation phenotypes of human umbilical cord mesenchymal cells dependent on adipogenic conditions. Exp Biol Med (Maywood). 2014;239(10):1340–1351.

54. Ali H, Al-Yatama MK, Abu-Farha M, Behbehani K, Al Madhoun A. Multi-lineage differentiation of human umbilical cord Wharton's jelly mesenchymal stromal cells mediates changes in the expression profile of stemness markers. PLoS One. 2015;10(10): e0122465.

55. Sotome S, Ae K, Okawa A, Ishizuki M, Morioka H, Matsumoto S, Nakamura T, Abe S, Beppu Y, Shinomiya K. Efficacy and safety of porous hydroxyapatite/type 1 collagen composite implantation for bone regeneration: a randomized controlled study. J Orthop Sci. 2016;21(3):373–380.

56. Nguyen PD, Lin CD, Allori AC, Schachar JS, Ricci JL, Saadeh PB, Warren SM. Scaffold-based rhBMP-2 therapy in a rat alveolar defect model: implications for human gingivoperiosteoplasty. Plast Reconstr Surg. 2009;124(6):1829–1839.

57. Mostafa NZ, Doschak MR, Major PW, Talwar R. Reliable critical sized defect rodent model for cleft palate research. J Craniomaxillofac Surg. 2014;42(8):1840–1846.

58. Nagamura-Inoue T, He H.Umbilical cord-derived mesenchymal stem cells: their advantages and potential clinical utility. World J Stem Cells. 2014;6(6):195–202.

59. Bugaighis I, Tiddeman B, Mattick CR, Hobson R. 3D comparison of average faces in subjects with oral clefts. Eur J Orthod. 2014;36(4):365–372.

60. Mahajan RK, Kaur A, Singh SM, Kumar P. A retrospective analysis of incidence and management of palatal fistula. Indian J Plast Surg. 2018;51(3):298–305.

61. Freitas JA, Almeida AL, Soares S, Neves LT, Garib DG, Trindade-Suedam IK, Yaedú RY, Lauris Rde C, Oliveira TM, Pinto JH. Rehabilitative treatment of cleft lip and palate: experience of the Hospital for Rehabilitation of Craniofacial Anomalies/ USP (HRAC/USP) – Part 4: oral rehabilitation. J Appl Oral Sci. 2013;21(3):284–292.

62. Gluckman E, Rocha V, Boyer-Chammard A, Locatelli F, Arcese W, Pasquini R, Ortega J, Souillet G, Ferreira E, Laporte JP, Fernandez M, et al. Outcome of cord-blood transplantation from related and unrelated donors. Eurocord transplant group and the European blood and marrow transplantation group. N Engl J Med. 1997;337(6):373–381.

63. Wang M, Yang Y, Yang D, Luo F, Liang W, Guo S, Xu J. The immunomodulatory activity of human umbilical cord blood-derived mesenchymal stem cells *in vitro*. Immunology. 2009; 126(2):220–232.

64. Shih IM. The role of CD146 (Mel-CAM) in biology and pathology. J Pathol. 1999;189(1):4–11.

65. Sorrentino A, Ferracin M, Castelli G, Biffoni M, Tomaselli G, Baiocchi M, Fatica A, Negrini M, Peschle C, Valtieri M. Isolation

and characterization of CD146+ multipotent mesenchymal stromal cells. Exp Hematol. 2008:36(8);1035–1046.

66. Shi S, Gronthos S. Perivascular niche of postnatal mesenchymal stem cells in human bone marrow and dental pulp. J Bone Miner Res. 2003;18(4):696–704.

67. Sacchetti B, Funari A, Michienzi S, Di Cesare S, Piersanti S, Saggio I, Tagliafico E, Ferrari S, Robey PG, Riminucci M, Bianco P. Self-renewing osteoprogenitors in bone marrow sinusoids can organize a hematopoietic microenvironment. Cell. 2007;131(2):324–336.

68. Dmitrieva RI, Minullina IR, Bilibina AA, Tarasova OV, Anisimov SV, Zaritskey AY. Bone marrow- and subcutaneous adipose tissue-derived mesenchymal stem cells: differences and similarities. Cell Cycle. 2012;11(2):377–383.

69. Russell KC, Phinney DG, Lacey MR, Barrilleaux BL, Meyertholen KE, O'Connor KC. In vitro high-capacity assay to quantify the clonal heterogeneity in trilineage potential of mesenchymal stem cells reveals a complex hierarchy of lineage commitment. Stem Cells. 2010;28(4):788–798.

70. Kang SD, Carlon TA, Jantzen AE, Lin FH, Ley MM, Allen JD, Stabler TV, Haley NR, Truskey GA, Achneck HE. Isolation of functional human endothelial cells from small volumes of umbilical cord blood. Ann Biomed Eng. 2013;41(10): 2181–2192.

71. Bowles KR, Tcw J, Qian L, Jadow BM, Goate AM. Reduced variability of neural progenitor cells and improved purity of neuronal cultures using magnetic activated cell sorting. PLoS One. 2019;14(3):e0213374.

72. Coskun H, Can A. The assessment of the in vivo to in vitro cellular transition of human umbilical cord multipotent stromal cells. Placenta. 2015;36(2):232–239.

73. Takahashi K, Tanabe K, Ohnuki M, Narita M, Ichisaka T, Tomoda K, Yamanaka S. Induction of pluripotent stem cells from adult human fibroblasts by defined factors. Cell. 2007; 131(15):861–872.

74. Carlin R, Davis D, Weiss M, Schultz B, Troyer D.Expression of early transcription factors Oct-4, Sox-2 and Nanog by porcine umbilical cord (PUC) matrix cells. Reprod Biol Endocrinol. 2006;4:8.

75. Jin HJ, Kwon JH, Kim M, Bae YK, Choi SJ, Oh W, Yang YS, Jeon HB. Downregulation of melanoma cell adhesion molecule (MCAM/CD146) accelerates cellular senescence in human umbilical cord blood-derived mesenchymal stem cells. Stem Cells Transl Med. 2016;5:427–439.

76. Kwon DY, Kwon JS, Park SH, Park JH, Jang SH, Yin XY, Yun JH, Kim JH, Min BH, Lee JH, Kim WD, et al. A computer-designed scaffold for bone regeneration within cranial defect using human dental pulp stem cells. Sci Rep. 2015;5:12721.

77. Zhang D, Gao P, Li Q, Li J, Li X, Liu X, Kang Y, Ren L. Engineering biomimetic periosteum with β-TCP scaffolds to promote bone formation in calvarial defects of rats. Stem Cell Res Ther. 2017;8(1):134.

78. Wang P, Liu X, Zhao L, Weir MD, Sun J, Chen W, Man Y, Xu HH. Bone tissue engineering via human induced pluripotent, umbilical cord and bone marrow mesenchymal stem cells in rat cranium. Acta Biomater. 2015;18:236–248.

79. Lohmann P, Willuweit A, Neffe AT, Geisler S, Gebauer TP, Beer S, Coenen HH, Fischer H, Hermanns-Sachweh B, Lendlein A, Shah NJ, et al. Bone regeneration induced by a 3D architectured hydrogel in a rat critical-size calvarial defect. Biomaterials. 2017;113:158–169.

80. Spicer PP, Kretlow JD, Young S, Jansen JA, Kasper FK, Mikos AG. Evaluation of bone regeneration using the rat critical size calvarial defect. Nat protoc. 2012;7(10):1918–1929.

81. Tsuchiya A, Sotome S, Asou Y, Kikuchi M, Koyama Y, Ogawa T, Tanaka J, Shinomiya K. Effects of pore size and implant volume of porous hydroxyapatite/collagen (HAp/Col) on bone formation in a rabbit bone defect model. J Med Dent Sci. 2008;55(1):91–99.

82. Chen W, Liu J, Manuchehrabadi N, Weir MD, Zhu Z, Xu HH. Umbilical cord and bone marrow mesenchymal stem cell seeding on macroporous calcium phosphate for bone regeneration in rat cranial defects. Biomaterials. 2013; 34(38):9917–9925.

83. Kargozar S, Mozafari M, Hashemian SJ, Brouki Milan P, Hamzehlou S, Soleimani M, Joghataei MT, Gholipourmalekabadi M, Korourian A, Mousavizadeh K, Seifalian AM. Osteogenic potential of stem cells-seeded bioactive nanocomposite scaffolds: a comparative study between human mesenchymal stem cells derived from bone, umbilical cord Wharton's jelly, and adipose tissue. J Biomed Mater Res B Appl Biomater. 2018;106(1):61–72.

84. Day AGE, Francis WR, Fu K, Pieper IL, Guy O, Xia Z. Osteogenic potential of human umbilical cord mesenchymal stem cells on coralline hydroxyapatite/calcium carbonate microparticles. Stem Cells Int. 2018;2018:4258613.

85. Dallas SL, Prideaux M, Bonewald LF. The osteocyte: an endocrine cell . . . and more. Endocr Rev. 2013;34(5):658–690.